

Diffuse spectral fundus reflectance measured using subretinally placed spectralon

David A. Salyer

University of Arizona
Optical Sciences Center
Tucson, Arizona 85721

Kurt R. Denninghoff

University of Arizona
Department of Emergency Medicine
and
Optical Sciences Center
Tucson, Arizona 85721

Neil Beaudry

University of Arizona
Optical Sciences Center
Tucson, Arizona 85721

Sreenivasa Basavanthappa

University of Arizona
Department of Ophthalmology
Tucson, Arizona 85721

Robert I. Park

University of Arizona
Department of Ophthalmology
and
Optical Sciences Center
Tucson, Arizona 85721

Russell A. Chipman

University of Arizona
Optical Sciences Center
Tucson, Arizona 85721

1 Introduction

Clinical diagnosis of ocular disease by observation of the ocular fundus began with the invention of the ophthalmoscope in 1851.¹ Introduction of spectrometric analysis of the ocular fundus provided a means of quantitatively recording the appearance of the fundus, leading to *in vivo* reflectometry being used to describe the physiological state of the fundus and to observe pathologic processes.²⁻⁴ Different investigators have used fundus reflectometry to measure the concentrations of ocular pigments such as melanin, xanthophylls, and hemoglobin in the retinal pigment epithelium, choroid, and retina.⁵⁻⁹ Detailed characterization of fundus reflectance is important for techniques such as fundus photography, photocoagulation, fluorescein angiography and retinal oximetry.

Several techniques have been developed to measure the reflectance of the fundus.^{5-7,9-18} Van Norren and Vos⁹ and Van

Abstract. The diffuse fundus reflectance and the spectral transmittance of the swine sensory retina was measured *in vivo* using intravitreal illumination. Pars plana vitrectomy and intravitreal manipulations were performed on a female American Yorkshire domestic swine. Light from a scanning monochromator was coupled into a fiber optic intraocular illuminator inserted into the vitreous. A 1.93-mm² region of the illuminated fundus was imaged from an oblique illumination angle. Multispectral retinal images were acquired for four experimental conditions: the eye (1) prior to vitrectomy, (2) after vitrectomy, (3) after insertion of a Spectralon disk super-retinally, and (4) after subretinal insertion of the disk. The absorption of melanin and hemoglobin in the red wavelengths was used to convert relative spectral reflectance to absolute reflectance. The flux scattered from the super-retinal Spectralon was used to correct for scattering in the globe. The transmittance of the sensory retina was measured *in vivo* using the scatter corrected subretinal Spectralon disk reflectance. The hemoglobin and melanin components of the spectrum due to scattered light were removed from the retinal transmission spectrum. The *in vivo* spectral transmittance of the sensory retina in this swine was essentially flat across the visible spectrum, with an average transmittance >90%. © 2008 Society of Photo-Optical Instrumentation Engineers. [DOI: 10.1117/1.2966953]

Keywords: spectroscopy; reflectance; ophthalmology.

Paper 07067R received Mar. 1, 2007; revised manuscript received Jan. 7, 2008; accepted for publication Feb. 19, 2008; published online Aug. 29, 2008.

Norren and Tiemeijer¹¹ measured the reflectance from the foveal and peripheral fundus and mathematically modeled the fundus. Their reflectance model was based on the Lambert-Beer law and used two reflective and four absorbing layers to describe the fundus. Their model provided stable results, but did not include a model for scattering effects. Delori and Pflibsen⁵ performed *in vivo* spectral reflectance measurements on human subjects with a wide range of fundus pigmentation and applied the model of van Norren and Tiemeijer.¹¹ Delori and Pflibsen⁵ also developed an alternate, more complex model that consisted of a scleral reflector, an absorbing-scattering layer meant to simulate the choroid, a blood layer, a melanin layer for the retinal pigment epithelium, and a spectrally flat reflector. They applied the equations of Kubelka and Munk to their data and achieved a better fit to measured spectra.⁵ Kubelka and Munk introduced a two-constant theory for the description of the reflectance properties of a material: the absorption coefficient and the scattering coefficient.¹⁹

Address all correspondence to: Kurt R. Denninghoff, University of Arizona, Department of Emergency Medicine, Tucson, AZ 85721; Tel: 520-626-1551; Fax: 520-626-2480; E-mail: kdenninghoff@aemrc.arizona.edu.

Delori's adaptation of the model of Kubelka and Munk treats the choroid as a diffuse absorbing scatterer backed by a reflecting sclera.⁵ Knighton and coworkers²⁰ measured the specular reflections from the inner limiting membrane of the retina of monkeys. Hammer et al.^{6,12} performed high spectral resolution studies with an imaging spectroscopy at high spatial resolution along a bar-shaped field on the retina. Hammer and Schweitzer⁶ developed a four-layer model to describe the reflectance of the ocular fundus: (1) the retina containing macular pigment in the foveal region, (2) the retinal pigment epithelium (RPE) pigmented with melanin, (3) the choroid containing blood and melanin, and (4) the sclera. The approach used for this model was the adding-doubling method as an approximate solution of the radiation transport equation for the reflectance. These previous methods to measure the fundus reflectance used extraocular illumination: the illumination came from outside of the eye. In most cases, the resulting fundus reflectance measurements included contributions of varying degrees from extraneous reflections from the anterior portion of the eye. Though the various layers of the retina were separated in the models used in these earlier works, no attempt was made to separate the reflectance of the layers of the retina empirically.

In this study, intravitreal illumination was used on a live swine eye with a super retinal or subretinal Spectralon (Labsphere, North Suttan, New Hampshire) disk to obtain *in vivo* fundus spectral reflectance measurements and sensory retina transmittance measurements. Intravitreal illumination is commonly used during retinal surgeries. Intravitreal illumination eliminated the influence of extraneous reflections from the cornea, lens, and vitreous to the reflectance measurements. To the authors' knowledge, this is the first known *in vivo* measurement of the isolated retinal reflectance.

2 Experimental Methods

Intravitreal surgery was performed on a 4-month-old female American Yorkshire domestic swine. The experimental protocol was approved by the University of Arizona Institutional Animal Care and Use Committee.

2.1 Surgical Procedure/Animal Preparation

The swine was administered a general anesthesia mixture consisting of air, nitrogen, oxygen, and isoflurane. A Swan-Ganz catheter was placed in the aorta just distal to the heart, and the second catheter was placed in the inferior vena cava just proximal to the heart. Blood samples collected from the two Swan-Ganz catheters were analyzed with an ISTAT Personal Clinical Analyzer (Heska Corporation, Fribourg, Switzerland) to monitor systemic arterial oxygen saturation (S_aO_2) and mixed venous oxygen saturation (S_vO_2). The SO_2 , PO_2 , PCO_2 , pH, and hematocrit were measured from the small blood samples. A peripheral oxygen saturation monitor was also placed in the rectum of the swine. A lid speculum was placed in the operative eye. The swine was inspired with 100% oxygen throughout the data collection.

A 4-mm infusion cannulum was placed through the pars plana and sutured in place. The infusion cannulum was attached to a balanced salt solution gravity feed system to maintain intraocular pressure. A contact vitrectomy lens (F36202.08, Bausch & Lomb, Rochester, New York) was

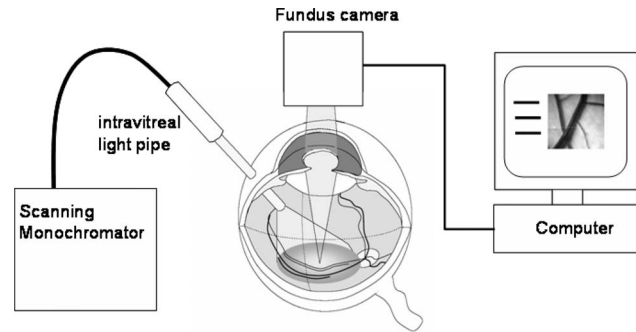


Fig. 1 Intravitreal illumination method for fundus reflectance measurements.

placed onto the cornea using an index matching (refractive index: $n_d=1.337$) viscoelastic coupling agent.

2.2 Fundus Imaging Apparatus and Data Collection

Following the surgical preparation of the animal, light from a scanning monochromator (Oriel Spectral Luminator, Irvine, California) was coupled into a fiber optic intravitreal illuminator (Alcon Laboratories, Fort Worth, Texas) that was inserted through the pars plana into the vitreous to illuminate the retina. The spectral resolution of the monochromator was approximately 10 nm. A 12-bit scientific grade charge-coupled device (CCD) camera (Hamamatsu Orca-AG, Hamamatsu, Japan) with a $3.3\times$ macro zoom lens was used to image the fundus. The peak wavelength of the 10-nm wavelength band was stepped from 420 to 700 nm, and an image of the target area was acquired at illumination center wavelengths of 420, 430, 440, 460, 480, 490, 500, 510, 521, 532, 540, 545, 548, 552, 555, 558, 561, 565, 570, 575, 580, 590, 600, 615, 630, 645, 660, 680, and 700 nm. Each camera exposure was triggered using a cardiac monitor (Digicare Life Windows, Boynton Beach, Florida) to minimize fundus thickness variations by acquiring all images at the same point during the cardiac cycle; retinal vessel diameter variations can range from 2% to 17% due to the cardiac cycle.²¹⁻²³ Additionally, the exposure time was adjusted to less than 40 ms (approximately 1/25 of the cardiac cycle) so the retinal blood vessel size should not vary appreciably during the exposure. The optical system is illustrated in Fig. 1.

Multispectral image sets were obtained over a $1.39\text{ mm} \times 1.39\text{ mm}$ region of the illuminated fundus of the intact eye. A dark image (obtained with the illuminator shutter closed) was subtracted from each image upon acquisition to correct for dark current and external light sources. The reflected light was collected over a solid angle of 0.028 sr, the solid angle subtended by the eye's pupil, which is the aperture stop of this system. After obtaining the spectral image set for the intact eye, the vitreous cutter was placed in the eye and a complete pars plana vitrectomy was performed.

After the postvitrectomy data was collected, a sclerotomy was created to allow the insertion of a small disk ($3\text{ mm} \times 1\text{ mm}$) of Spectralon. The Spectralon was placed on top of the fundus area previously imaged and spectral images were obtained. A retinal detachment was induced near the site of the postvitrectomy measurements and the Spectralon disk was inserted underneath the retina and the transmittance of the

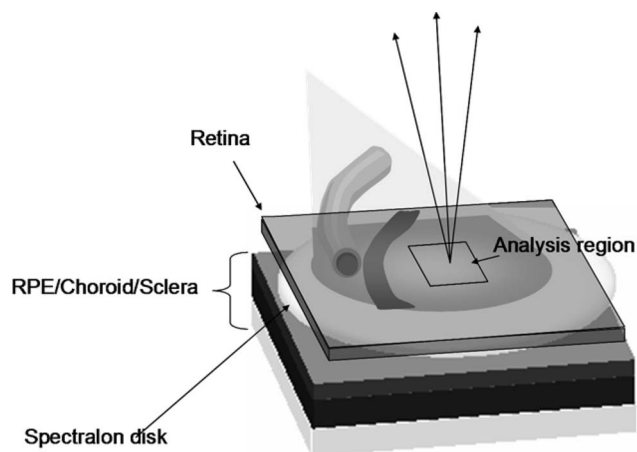


Fig. 2 A retinal detachment was induced using perfluoron and a small, thin Spectralon disk was carefully inserted between the retina and RPE.

isolated retina was measured for the same field of view. Figure 2 shows a drawing of the placement of the subretinal Spectralon chip.

2.3 Data Calibration and Image Alignment

A calibration data set was collected by measuring the output port of an integrating sphere illuminated with the fiber optic illuminator. The multispectral images were corrected for spectral variation in the light source and the spectral response of the CCD by dividing by the calibration spectrum. The inner wall of the integrating sphere is coated with Spectralon, which has a very uniform spectral reflectivity and is commonly used as a calibration standard.²⁴

The fundus multispectral image sets were registered to correct for any relative motion between the swine fundus and the imaging camera that occurred during data collection. Images were aligned to within a fraction of a pixel using a bicubic spline interpolation in conjunction with a maximum mutual information merit function algorithm.²⁵

2.4 Image Processing and Data Analysis Techniques

Three sites relatively free of large vessels were chosen for analysis of fundus reflectance as indicated by the squares in Fig. 3. Multispectral image sets were acquired for the following four experimental conditions: (1) from the intact eye, (2) from the eye postvitrectomy, (3) after insertion of subretinal Spectralon, and (4) for super-retinal Spectralon. The spectrum

was calculated for each condition by averaging the flux over a small region (100 × 100 microns) of the fundus shown in Fig. 3 for each of the 29 monochromatic images.

The signal recorded by the CCD camera is a product of the spectral irradiance of the light source, the spectral response of the imaging system, and the spectral transmittance or reflectance of any structures that may interact with the light captured by the imaging system. This relationship is expressed in equation form for each of the four experimental conditions described in the previous paragraph (denoted S_{IE} , S_{PE} , S_{sub} , and S_{super} , the signal recorded for experimental conditions 1 through 4, respectively) as follows:

$$S_{IE}(\lambda) = P_{IE} * \Theta(\lambda) * R_{fundus}(\lambda), \quad (1)$$

$$S_{PE}(\lambda) = P_{PE} * \Theta(\lambda) * R'_{fundus}(\lambda), \quad (2)$$

$$S_{sub}(\lambda) = P_{sub} * \Theta(\lambda) * T_{SR}(\lambda) * R''_{fundus}(\lambda) * R_{Spectralon}, \quad (3)$$

$$S_{super}(\lambda) = P_{super} * \Theta(\lambda) * R_{Spectralon} * R''_{fundus}(\lambda). \quad (4)$$

$P_i * \Theta(\lambda)$ is a multiplicative term describing the spectral irradiance distribution of the illumination and the spectral response of the imaging system. P_i refers to the four absolute irradiance constants P_{IE} , P_{PE} , P_{sub} , and P_{super} . $\Theta(\lambda)$ is measured during calibration and provides the relative spectral irradiance of the light illuminating a particular region of the fundus for each experimental condition. Light exits the fiber optic illuminator with a numerical aperture of 0.655 in the vitreous; thus this parameter is different for each spatial position in a spectral image set. P_i was not directly measured; the calibration process only measures $\Theta(\lambda)$, the relative spectral power distribution. P_i was calculated for each of the experimental conditions, and the results are included in the paper. The remaining terms are defined as follows: $R_{fundus}(\lambda)$ is the fundus reflectance, $R'_{fundus}(\lambda)$ is the fundus reflectance after vitrectomy, $T_{SR}(\lambda)$ is the transmittance of the sensory retina in double pass, $R_{Spectralon}$ is the reflectance of the Spectralon disk, and $R''_{fundus}(\lambda)$ is the reflectance of the fundus not shadowed by the Spectralon chip. Values for $T_{OM}(\lambda)$ were obtained from van de Kraats et al.²⁶ The Lambertian reflectance of the Spectralon chip is constant with wavelength: $R_{Spectralon}$ is equal to 0.91 for a 1-mm thick piece of Spectralon.²⁷

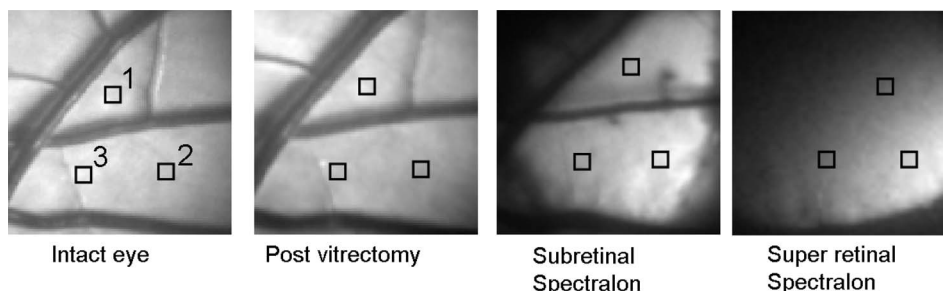


Fig. 3 The 523-nm image for each of the 4 experimental conditions is shown. Reflectance spectra were averaged over each of the squares.

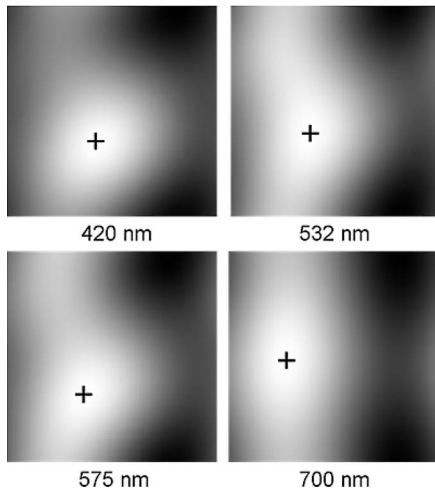


Fig. 4 Four low pass filtered images of the intact eye. The small cross on each image marks the location of the maximum intensity, corresponding to the axis of the fiber optic illuminator, or the peak intensity of the incident cone of light. The location of the maximum intensity moves as the swine breathes.

2.4.1 Low pass filtering and light/fundus relative motion correction

Despite attempts to immobilize the swine’s head during data collection, small relative motion between the illumination beam and the fundus occurred as a result of the swine’s breathing. This motion is in addition to the relative motion between the fundus and the camera, which was corrected for using the maximization of the mutual information as described in Sec. 2.3. Low pass filtered images (Fig. 4) reveal the relative motion between the illumination and the swine

fundus; although the physical structures of the fundus were aligned for all the spectral images, the location of the peak illumination region varied among the spectral images. Figure 4 shows four low pass filtered images (420, 523, 560, and 680 nm) obtained for the intact eye.

To analyze the motion of the illuminating beam, frequency domain filtering with a Gaussian low pass filter was performed on each of the monochromatic images. The filter, $H(\xi, \eta)$, is a Gaussian low pass filter with a spatial domain kernel size of 56 pixels for a 102×102 pixel image (full width at half maximum=56 pixels),

$$H(\xi, \eta) = \exp - \left[\frac{\left(\xi - \frac{N}{2}\right)^2 + \left(\eta - \frac{N}{2}\right)^2}{(2\sigma)^2} \right]. \quad (5)$$

Given the Fourier transform of the image $i(\xi, \eta)$

$$i(\xi, \eta) = \frac{1}{N^2} \sum_{x=1}^{N-1} \sum_{y=1}^{N-1} I(x,y)^* \exp \left[-i2\pi \left(\frac{\xi x}{N} + \frac{\eta y}{N} \right) \right], \quad (6)$$

the low pass filtered image, $I_{filtered}(x,y)$,

$$I_{filtered}(x,y) = F^{-1} \{ H(\xi, \eta) * i(\xi, \eta) \}, \quad (7)$$

provides the centroid of the illumination as shown in Fig. 4. Figure 5 shows the frequency [Fig. 5(a)] and spatial domain [Fig. 5(b)] representation of the filter $H(\xi, \eta)$.

The beam centroid motion as a function of illumination wavelength is determined from the filtered images. This small relative motion causes irradiance fluctuations leading to errors in the measured spectrum. An algorithm was developed to correct for the motion of the illuminating irradiance: (1) for the filtered reference image (the 552-nm image), the ratio

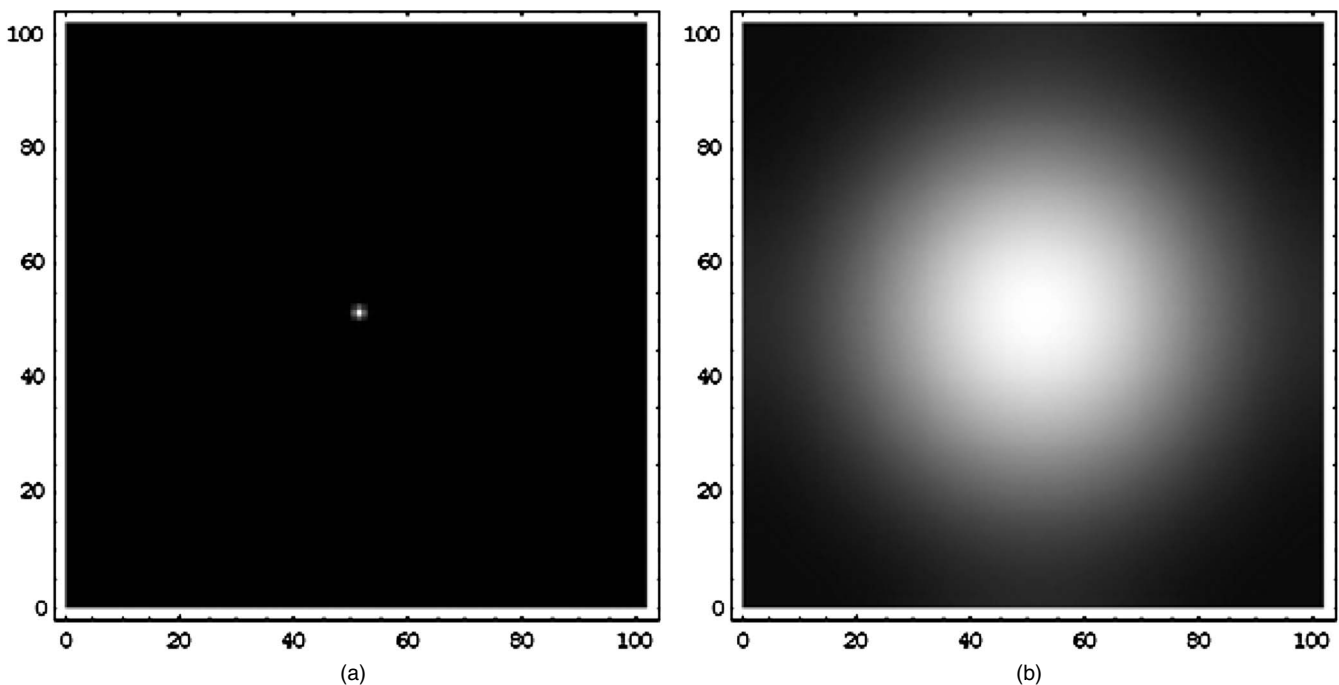


Fig. 5 Low pass filter in the (a) frequency and (b) spatial domains.

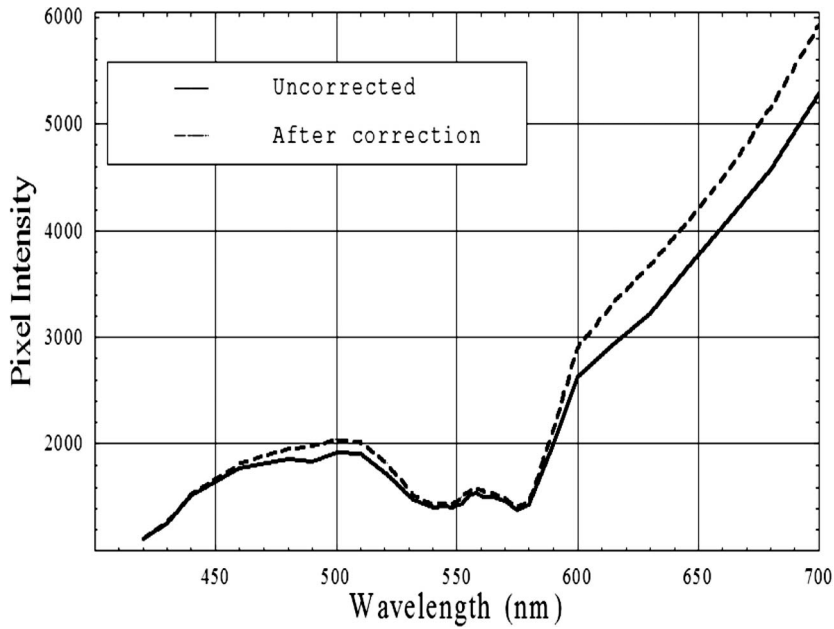


Fig. 6 An example of the effect of illumination motion correction. The solid line is the signal recorded by the CCD, and the dashed line shows motion-corrected spectra.

between the maximum of the image and the value at the analysis site is calculated; (2) the corresponding ratios are determined for all the filtered images in the spectral image set; and (3) a correction factor, $c.f. = r_{base}/r_{test}$, is applied to the reflectance measured at the illumination site for each spectral image. The assumption is that the illumination profile does not change appreciably over the visible spectrum. Figure 6 illustrates the motion correction for one of the reflectance curves.

2.4.2 Relative spectral fundus reflectance

Using Eqs. (1)–(4), the relative fundus reflectance can be estimated to within the multiplicative constant P_i for the four experimental conditions (relative spectral values denoted by script symbols):

$$\mathcal{R}_{fundus}(\lambda) = P_{IE} * R_{fundus}(\lambda) = \frac{S_{IE}(\lambda)}{\Theta(\lambda)}, \quad (8)$$

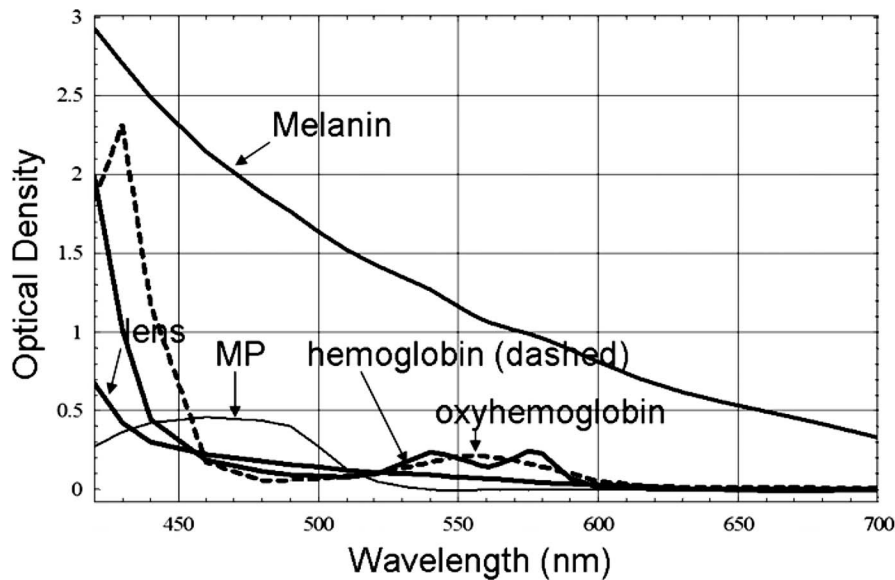


Fig. 7 Optical density of the dominant spectrally absorbing constituents of the eye (Refs. 26 and 31).

$$\mathcal{R}'_{fundus}(\lambda) = P_{PE} * R'_{fundus}(\lambda) = \frac{S_{PE}(\lambda)}{\Theta(\lambda)}, \quad (9)$$

$$\mathcal{T}_{SR}(\lambda) = P_{sub} * T_{SR}(\lambda) = \frac{S_{sub}(\lambda)}{\Theta(\lambda) * R_{Spectralon} * R''_{fundus}(\lambda)}, \quad (10)$$

$$\mathcal{R}''_{fundus}(\lambda) = P_{super} * R''_{fundus}(\lambda) = \frac{S_{super}(\lambda)}{\Theta(\lambda) * R_{Spectralon}}. \quad (11)$$

2.4.3 Power compensation: estimation of absolute reflectance

The constant term P_i in Eqs. (1)–(4) was calculated to provide the absolute fundus reflectance and sensory retina transmittance. A calculation of P_i is described for the intact eye; the other three conditions were similarly analyzed.

By taking the logarithm of Eq. (1), a set of linear equations for all λ_i is formed

$$\log_{10} \left[\frac{S_{IE}(\lambda)}{\Theta(\lambda) * T_{OM}(\lambda)} \right] = \log_{10}[P_{IE}] + \log_{10}[R_{fundus}(\lambda)], \quad (12)$$

where all known terms are grouped on the left-hand side and $T_{OM}(\lambda)$ is the transmittance of the ocular media. An appropriate model of $R_{fundus}(\lambda)$ provides an overdetermined set of linear equations used to solve for P_{IE} . $R'_{fundus}(\lambda)$, $T_{SR}(\lambda)$, and $R''_{fundus}(\lambda)$ are similarly modeled and the resulting linear equations solved for P_i . A fundus reflectance model, Eq. (13), is used to model the measured quantity for all four experimental conditions based on the assumption that a finite number of reflecting, transmitting, and absorbing layers with known spectral extinction coefficients shape the spectral profile of light reflecting from the fundus. The primary ocular constituents that contribute to the spectrum are the ocular media (lens, cornea), hemoglobin, and melanin, although several other absorbers in smaller concentrations are likely to be present.^{5,26} The reflectance model is

$$R_{fundus}(\lambda) = T_{OM}(\lambda) * A_{Hb}(\lambda) * A_M(\lambda) * A_{MP}(\lambda), \quad (13)$$

where $T_{OM}(\lambda)$ is the transmittance of the ocular media, $A_{Hb}(\lambda)$ is absorption due to blood (and is dependent on the

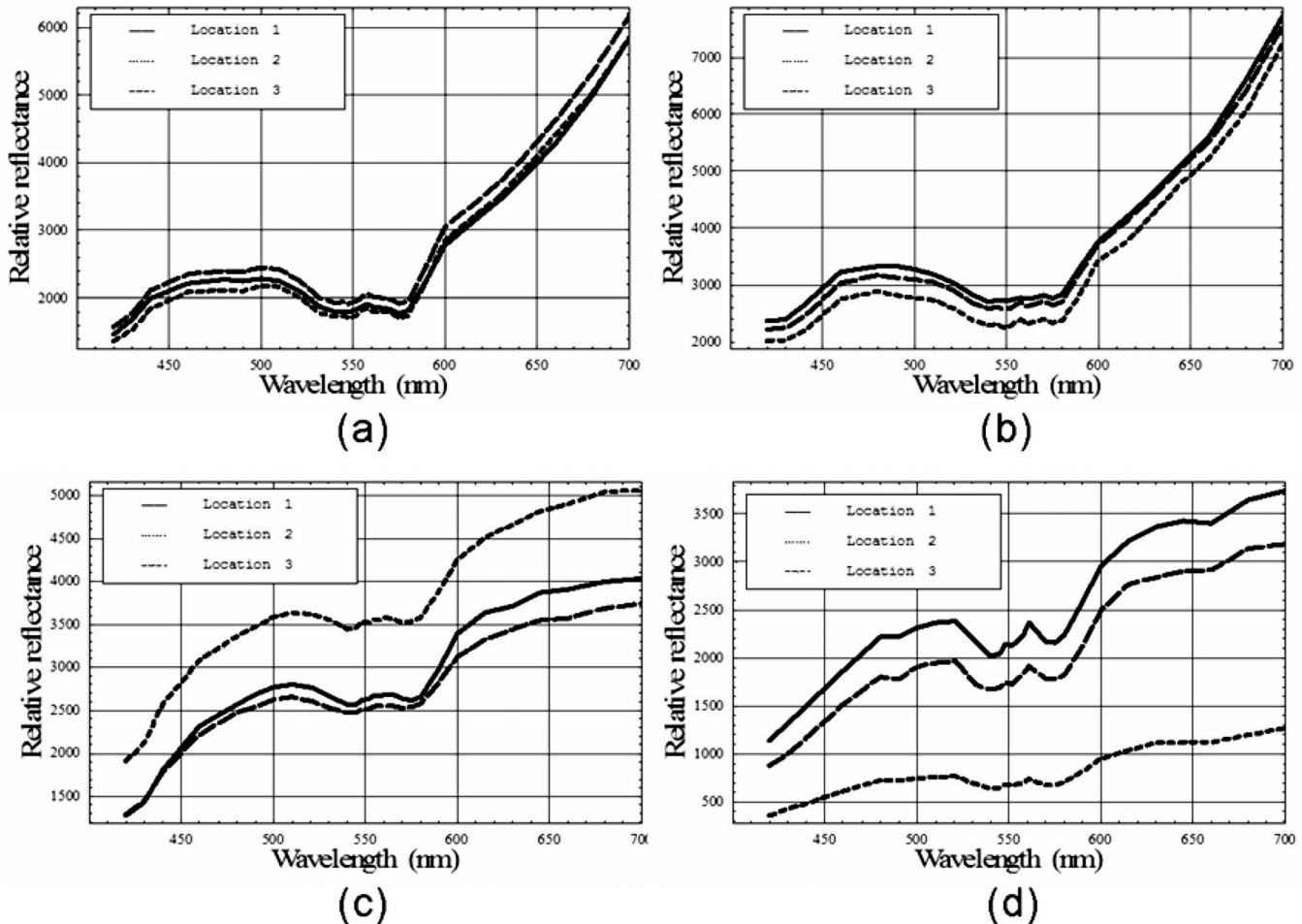


Fig. 8 Relative reflectance measurements for the (a) intact eye, (b) postvitrectomy, (c) subretinal Spectralon, and (d) super-retinal Spectralon.

Table 1 Amounts of hemoglobin and melanin absorption and the P_i parameter for the four conditions and three locations. The $c \cdot d$ product gives a measure of the amount of blood at a test site, the Y term indicates the amount of melanin, and the P_i parameter is proportional to the incident flux at each analysis site.

Power Correction Algorithm Results							
Intact Eye				Postvitrectomy			
	$c \cdot d$	Y	P		$c \cdot d$	Y	P
Location 1	0.004884	0.669	9386	Location 1	0.002790	0.649	13489
Location 2	0.007047	0.655	9379	Location 2	0.002478	0.682	12990
Location 3	0.005425	0.644	9770	Location 3	0.001647	0.634	13023
Average	0.006	0.656	9512	Average	0.002	0.655	13167
Standard Deviation	0.001	0.013	224	Standard Deviation	0.001	0.024	279
Subretinal Spectralon				Super retinal Spectralon			
	$c \cdot d$	Y	P		$c \cdot d$	Y	P
Location 1	0.004911	0.221	76096	Location 1	0.007423	0.157	59206
Location 2	0.003611	0.175	88136	Location 2	0.009393	0.182	46814
Location 3	0.003323	0.231	71605	Location 3	0.007606	0.147	46284
Average	0.004	0.209	78612	Average	0.008	0.162	50768
Standard Deviation	0.001	0.030	8548	Standard Deviation	0.001	0.018	7312

oxygen saturation), $A_M(\lambda)$ is absorption due to melanin, and $A_{MP}(\lambda)$ is the absorption due to macular pigments. Figure 7 illustrates the absorption curves.

Examination of Fig. 7 shows that for the wavelength range of 575 to 700 nm, the only components with substantial absorption are melanin and blood. Using the fundus reflectance model in the aforementioned wavelength range, Eq. (12) can then be rewritten to include the fundus reflectance model as

$$\hat{D}_{IE}(\lambda) = \hat{P}_{IE} + \hat{A}_{Hb}(\lambda) + \hat{A}_M(\lambda),$$

$$\hat{A}_{Hb}(\lambda) = \varepsilon_{Hb}(\lambda) * c * d,$$

$$\hat{A}_M(\lambda) = M(\lambda) * Y, \tag{14}$$

where $\hat{D}_{IE}(\lambda)$ represents the left-hand side of Eq. (12). The optical density due to blood is \hat{A}_{Hb} (the “*” symbol denotes base 10 logarithm) and is described by the product of the millimolar extinction coefficient (ε_{Hb}), the concentration of hemoglobin (c), and the effective interaction path length (d). The oxygen saturation of the blood in each of the four cases was calculated using the method described by Denninghoff

et al.²⁸ to be 85%, 52%, 92%, and 92% for the four cases and the corresponding millimolar extinction coefficients were used in Eq. (14). \hat{A}_M is the optical density due to melanin (found mainly in the RPE), which is a product of M , the millimolar extinction coefficient and the relative concentration of melanin (Y). Writing Eq. (14) for the illumination wavelengths from 575 to 700 nm provides a set of overdetermined linear equations that was solved using the pseudo-inverse technique to provide the least-squares solution for P_i .

3 Experimental Results

Relative and absolute fundus reflectance spectra are presented in this section for the three analysis sites indicated in Fig. 3.

3.1 Diffuse Relative Reflectance Measurements

Figure 8 shows the measured relative fundus reflectance for the four experimental conditions. Figures 8(a) and 8(b) show similar behavior for the intact eye and the postvitrectomy data: reflectance is lowest in the blue light and increases until 510 nm for the intact eye and 480 nm for postvitrectomy. Oxyhemoglobin is evident by the appearance of bimodal local minima at 542 and 576 nm; these minima correspond to the absorption maxima of oxyhemoglobin. The reflectance

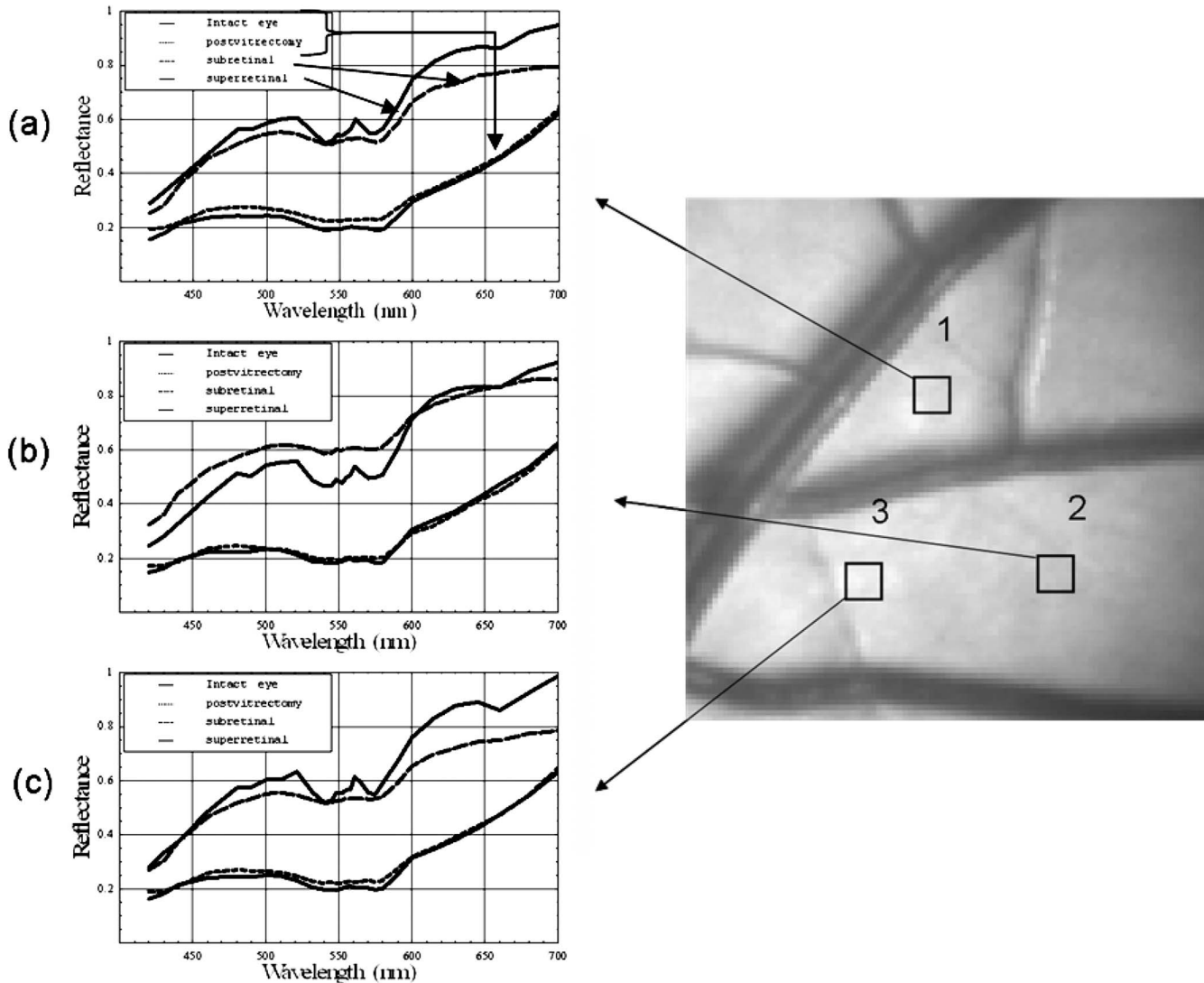


Fig. 9 Absolute reflectance measurements at the three analysis locations [(a) to (c)] after correction for motion and power of the illuminating beam. In each plot, the separate curves correspond to the four experimental conditions. The super-retinal spectrum contains two components: (1) light that reflects from the Spectralon and (2) light that has also scattered from the globe and into the imaging system. The latter contribution contains a strong hemoglobin signature.

increases by a factor of approximately 6 for all three curves in each plot in the 420- to 700-nm range, and by a factor of approximately 2 for the 590- to 700-nm range. Figures 8(c) and 8(d) show markedly different behavior, although some similarities exist. For both the sub- and super-retinal Spectralon, a local maximum exists at 510 nm, and again, the oxyhemoglobin absorption spectrum is evident. The reflectance in this case, however, increases by a factor of approximately 4 in the 420- to 700-nm range, and a factor of approximately 1.75 in the 590- to 700-nm range.

3.2 Absolute Diffuse Relative Reflectance Measurements

Using the technique described in Sec. 2, the relative reflectance data was converted to absolute reflectance by solving for the P_i coefficients from Eqs. (8) to (11). The results for the

reflectance curves measured at the three analysis sites are included in Table 1, and the power corrected curves are shown in Fig. 9.

The relative melanin Y values calculated for the intact eye and the postvitrectomy eye are much larger than the corresponding Spectralon values for all three locations in the data. This behavior is to be expected: The light striking both the subretinal and super-retinal Spectralon should see only a small fraction of the melanin encountered for the first two conditions. In fact, the only optical path for melanin absorption in the super-retinal Spectralon data is scattered light from the globe. The values obtained for the oxyhemoglobin $c \cdot d$ products correspond to a blood thickness interaction of 40 to 100 μm .

The absolute reflectance data shown in Fig. 9 is arranged such that the stacked plots in the left-hand column display the

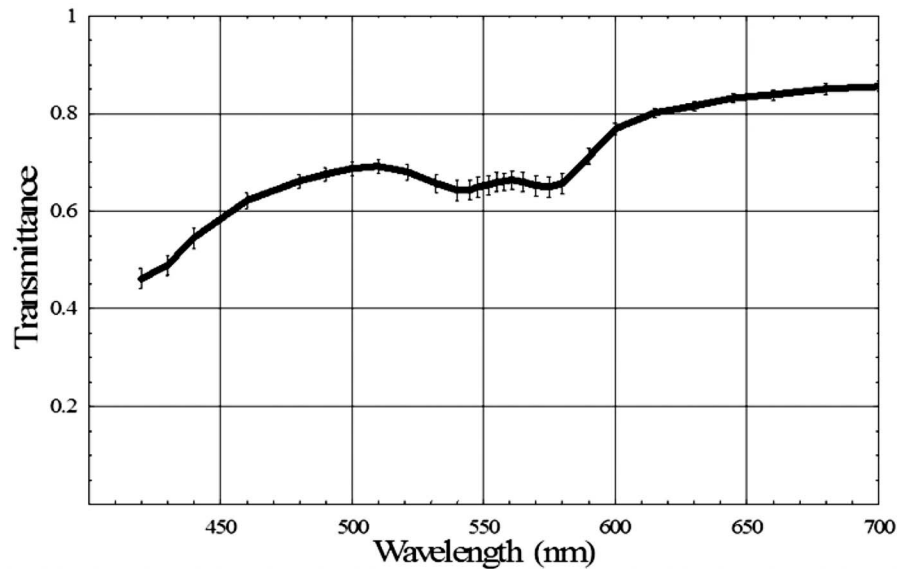


Fig. 10 Single pass transmittance of the sensory retina, averaged over the three locations measured from the subretinal Spectralon. The illumination component from light scattered from the globe acquired a strong hemoglobin signature, which overestimated the amount of blood contained in the sensory transmittance.

data from the three analysis sites. For all three locations, the reflectance for the first two cases is similar (intact eye and postvitrectomy), with the primary difference between the two curves being a difference in oxygen saturation (measured at 85% and 52%, respectively). The reflectance is approximately 17% at 420 nm, rises to local maxima of approximately 25% at 497 and 485 nm for the intact eye and postvitrectomy eye, respectively. From there, both curves decrease to bimodal local minima at 542 and 576 nm, and then increase monotonically from a value of $\approx 30\%$ at 590 nm to $\approx 60\%$ at 700 nm.

The Fig. 9 plots for subretinal Spectralon show more variation, ranging from a reflectance of $\approx 19\%$ to 25% at 420 nm. Above this wavelength, the reflectance increases to a local maximum of $\approx 48\%$ to 62% at 500 nm. The characteristic bimodal maxima are located at 542 and 576 nm. The reflectance again increases from the 575- to 700-nm range by 55% to 62% for 575 nm to 75% to 80% for 700 nm. The super-retinal Spectralon spectrum contains considerably more noise than the other spectra, possibly due to less exposure time in response to high reflectivity. The super-retinal Spectralon should be the highest recorded reflectance spectra in all three cases of Fig. 9, but in Fig. 9(b) was corrected to a value lower than that of the subretinal Spectralon data. This is likely due to the failure of our power fluctuation compensation method to completely match the power in the region and noise combined with the very high transmission of the sensory retina. In most cases [Figs. 9(a)–9(c)], however, the super-retinal Spectralon had a higher reflectance than the subretinal Spectralon.

The transmittance of the sensory retina in a single pass can be obtained by taking the square root of the subretinal Spectralon data in Fig. 9, which were acquired in double passes. Figure 10 represents the transmittance of the sensory retina averaged over all three locations based on the power-corrected Eq. (10). The spectrum overestimates the influence of both melanin and hemoglobin due to scattered light from the globe. Equation (11) was used to calibrate for this scat-

tered light term. The super-retinal spectrum calibrates the transmission through the anterior chamber and the scattered light from the globe itself. The latter component contains a significant hemoglobin signature. By dividing Eq. (10) by Eq. (11), the scatter corrected *in vivo* transmittance of the sensory retina is obtained (Fig. 11),

$$T(\lambda) = \frac{P_{sub} * T_{SR}(\lambda)}{P_{super} * R''_{fundus}(\lambda)}. \quad (15)$$

Figure 12 displays the expected transmittance of the sensory retina, which is nearly flat across the visible spectrum with an absolute transmittance $>90\%$ for all wavelengths.

4 Discussion

In our experimental design, we carefully matched the power delivery and detection systems so that the power delivered and detected at any given wavelength was normalized to all the others. This allowed us to use a simplified model equation that did not directly account for wavelength-dependent scattering as long as the power determinations were accurate for a reasonable region of the spectra. Because the model we used allowed us to fit the same area of the visible spectrum (the red region) in all of our experimental conditions, we were satisfied that we could use the results to normalize power as described. The absorption of the components of the retina and the scattering of the structures of the retina are nearly constant in the red wavelengths, making our assumptions required for the model fit valid in this region. The behavior of light in the blue-green wavelength range was unexpected. The reflectance is much larger in the blue-green spectrum than can be explained based on the ocular absorbers modeled here, as was indicated in Fig. 13 where the logarithm of the reflectance is shown superposed with the calculated reflectance determined using the relative contributions of melanin and hemoglobin.

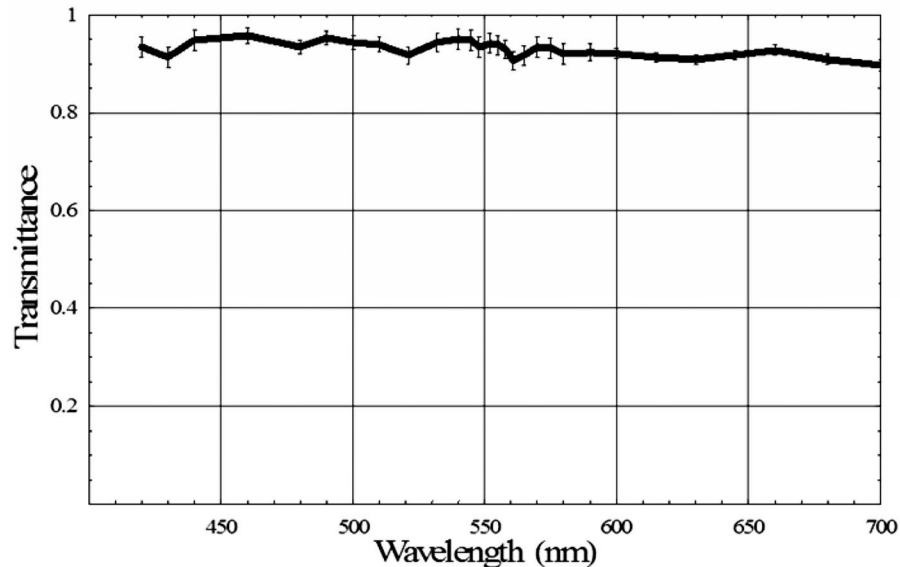


Fig. 11 Single pass transmittance of the sensory retina, averaged over the three locations measured from the subretinal Spectralon data and corrected for the influence of scattered light using the super-retinal data.

The fit is very good for wavelengths longer than 550 nm, but the reflectance is much larger than predicted in the blue-green region. One way to explain this discrepancy is to hypothesize a component of the retina anterior to the RPE that reflects more light as the wavelength decreases below 550 nm. Changes in scattering with wavelength and the resulting change in relative pathlength are also possible explanations for the mismatch between our model and the observed spectrum in the blue-green region. Because the discrepancy is much larger in the intact and postvitrectomy eye, these reflections must be occurring posterior to the sensory retina. We can only support this interesting finding with data from one animal eye; further research is required prior to any significant conclusions about the swine fundus reflectance in the blue-green region.

Our goal was to measure the reflectance of the sensory retina isolated from the underlying components to inform systems that use the reflected light to analyze *in vivo* signals that traverse the sensory retina prior to reaching or returning from underlying structures. An example of such a system is optical

coherence tomography (OCT), which isolates the light that is backscattered prior to reaching the pigment epithelium. Our result seems to indicate that OCT using light that is highly absorbed by the RPE such as blue or green wavelengths would remain feasible for interrogating the sensory retina because the reflectance/transmittance of this structure is nearly spectrally neutral.

The absolute swine fundus reflectance in this paper is significantly higher than the human fundus reflectance found by other authors, although the spectral shape is similar.^{9,29,30} The explanation for this difference may lie in the illumination and imaging method used in our study. The flux from a point on the fundus is integrated over a solid angle determined by the dilated pupil of the swine; if this solid angle is larger than the solid angle in other measurements, the measured reflectivity will be correspondingly larger. Also, diffuse illumination is used adding a large amount of scattered light to the measured signal, resulting in two primary light sources: The direct light from the fiber optic illuminator, and a glowing “integrating sphere” of illumination arising from scattered light from the entire globe. The relative intensity of this second “source” is highly dependent on the illumination technique and a stray light model of the eye might provide an estimate of the magnitude of the contribution for a given illumination method. Obtaining reflectance data from the eye using diffusely illuminating light sources as is done with fundus cameras creates scattered light signals from within the globe that are similar in magnitude to the integrating sphere effect we observed. Further, systems that use small illuminating spots such as the strictly localized orbital will still have a scatter signal from within the globe but the signal will be relatively attenuated. This provides an advantage to laser scanning systems when performing tests that attempt to quantify the amount of individual chromophores in a given area of the retina. The commonly used oximetry technique where the reflected light from the perivascular region is divided into the reflected light from the vessel should account for the integrating sphere effect by

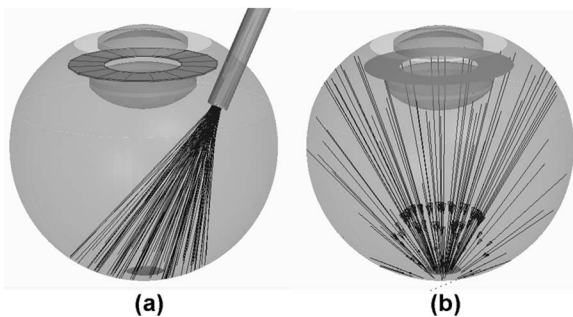


Fig. 12 The measurement area is illuminated by two mechanisms: (1) illumination provided directly from the fiber optic illuminator and (2) scattered light from the globe that behaves like an integrating sphere illuminator.

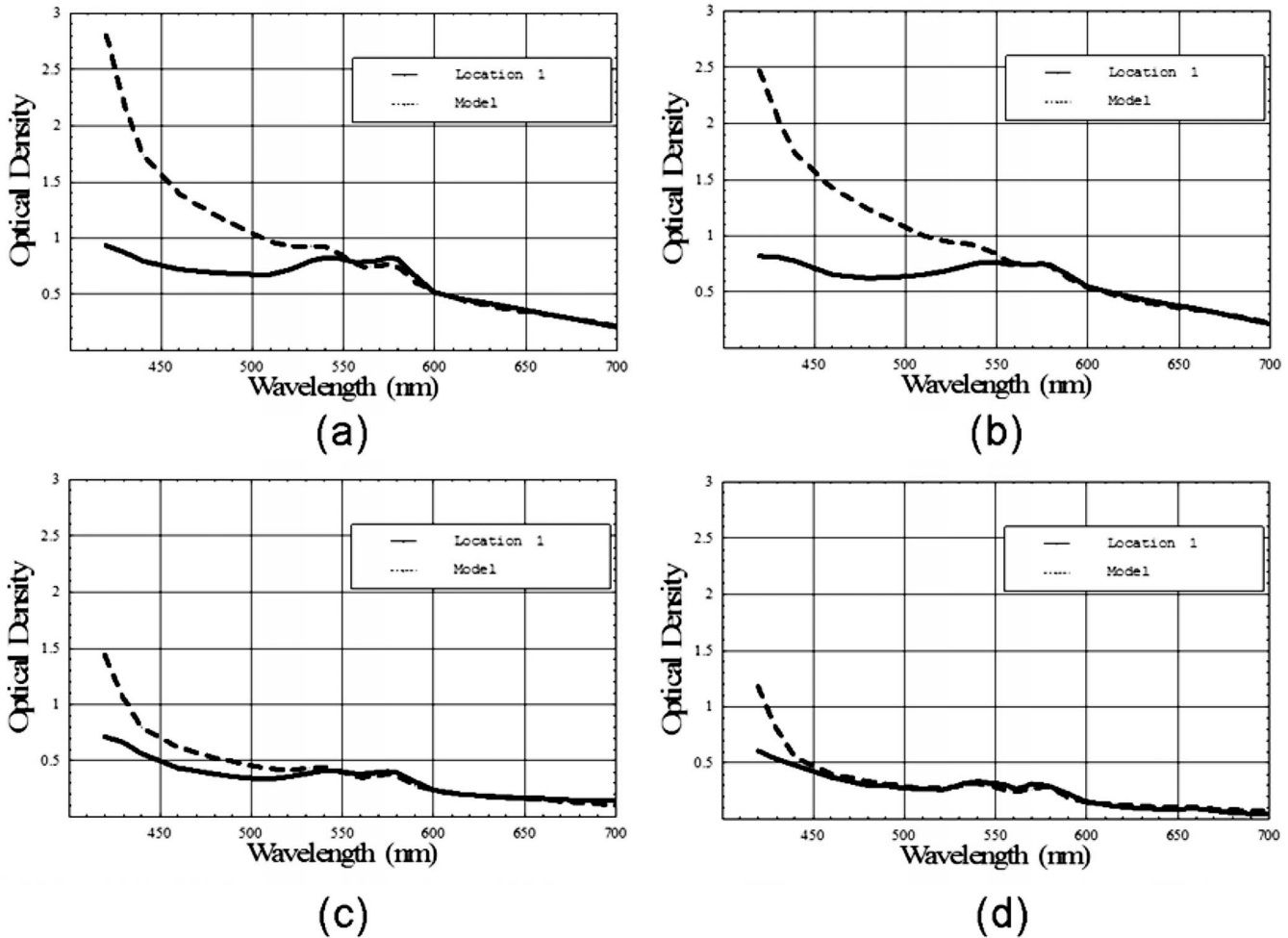


Fig. 13 Measured reflectance versus the predicted reflectance based on Eq. (12) for (a) the intact eye, (b) the postvitrectomy eye, (c) the subretinal Spectralon, (d) and the super-retinal Spectralon. These spectra suggest the presence of a blue-green reflector in the retina above the RPE.

dividing out the signal. The requirement to use the perivascular fundus signal in this manner has led to the dependence of calibrated oximetry on the absolute fundus reflectance in the perivascular region.³¹⁻³³

5 Summary and Conclusions

We have demonstrated the first *in vivo* sensory retina transmittance and fundus reflectance measurements that were acquired using subretinal Spectralon as a calibration target. The scattered light throughout the globe behaves like an integrating sphere, and this physical phenomenon should be included in retinal spectroscopy model equations. Intravitreal illumination effectively removed the reflections arising from the anterior interfaces of the swine eye. Evidence for a blue-green reflector above the RPE is presented.

Any conclusions regarding retinal behavior from this study are limited because we only studied one eye *in vivo*. However, the techniques used to carry out the experiment are novel. These results warrant further study, including quantifying pigmentation contributions, reflectance changes, and retinal thickness when different eyes and different locations are studied. The effects of age, disease states, and therapies might also be studied using this technique.

References

1. H. Helmholtz, "Beschreibung eines Augenspiegels zur Untersuchung der Netz haut im lebenden Auge," *Arch. Physiol. Heilk.* **11**, 827-830 (1851).
2. D. Schweitzer, S. Guenther, M. Scibor, and M. Hammer, "Spectrometric investigation in ocular hypertension and early stages of primary open angle glaucoma and of low tension glaucoma—multisubstance analysis," *Int. Ophthalmol.* **16**, 251-257 (1992).
3. D. Schweitzer, S. Klein, S. Guenther, and M. Hammer, "Early diagnosis of glaucoma by means of fundus reflectometry," *New Trends Ophthalmol* **7**, 241-247 (1992).
4. R. W. Knighton, S. G. Jacobson, and C. M. Kemp, "The spectral reflectance of the nerve fiber layer of the macaque retina," *Invest. Ophthalmol. Visual Sci.* **30**, 2393-2402 (1989).
5. F. C. Delori and K. P. Pflibsen, "Spectral reflectance of the human ocular fundus," *Appl. Opt.* **28**, 1061-1077 (1989).
6. M. Hammer and D. Schweitzer, "Quantitative reflection spectroscopy at the human ocular fundus," *Phys. Med. Biol.* **47**, 179-191 (2002).
7. W. Hunold and P. Malessa, "Spectrophotometric determination of melanin pigmentation of the human ocular fundus *in vivo*," *Ophthalmic Res.* **6**, 355-362 (1974).
8. G. S. Brindley and E. N. Willmer, "The reflection of light from the macular and peripheral fundus oculi in man," *J. Physiol. (London)* **116**, 350-356 (1952).
9. D. van Norren and J. J. Vos, "Spectral reflectance of the human eye," *Vision Res.* **26**, 313-320 (1986).
10. J. J. Vos, A. A. Munnik, and J. Boogaard, "Absolute spectral reflectance of the fundus oculi," *J. Opt. Soc. Am.* **55**, 573-574 (1965).

11. D. van Norren and T. Tiemeijer, "Spectral reflectance of the human eye," *Vision Res.* **26**, 313–320 (1978).
12. M. Hammer, D. Schweitzer, L. Leistritz, M. Scibor, K-H Donnerhacke, and J. Strobel, "Imaging spectroscopy of the human ocular fundus *in vivo*," *J. Biomed. Opt.* **2**(4), 418–425 (1997).
13. F. C. Delori, "Spectrophotometer for noninvasive measurement of intrinsic fluorescence and reflectance of the ocular fundus," *Appl. Opt.* **33**, 7439–7452 (1994).
14. F. C. Delori and S. A. Burns, "Fundus reflectance and the measurement of crystalline lens density," *J. Opt. Soc. Am. A* **13**(2), 215–226 (1996).
15. N. P. A. Zagers, J. van de Kraats, T. T. J. M. Berendschot, and D. van Norren, "Simultaneous measurement of foveal spectral reflectance and cone-photoreceptor directionality," *Appl. Opt.* **41**(22), 4686–4696 (2002).
16. G. J. van Blockland, "Directionality and alignment of the foveal receptors, assessed with light scattered from the human fundus *in vivo*," *Vision Res.* **26**(3), 495–500 (1986).
17. A. E. Eisner, S. A. Burns, G. W. Hughes, and R. H. Webb, "Reflectometry with the scanning laser ophthalmoscope," *Appl. Opt.* **31**, 3697–3710 (1992).
18. R. W. Knighton, "Quantitative reflectometry of the ocular fundus," *IEEE Eng. Med. Biol. Mag.* **14**, 43–51 (1995).
19. G. Kortum, *Reflectance Spectroscopy, Principles, Methods, Applications*, Springer-Verlag, New York, pp. 116–120 (1969).
20. R. W. Knighton, S. G. Jacobson, and M. I. Roman, "Specular reflection from the surface of the retina," in *SPIE Laser Surgery: Advanced Characterization, Therapeutics, and Systems, Proc. SPIE* **1066**, 10–17 (1989).
21. M. D. Knudtson, B. E. K. Klein, R. Klein, T. Y. Wong, L. D. Hubbard, K. E. Lee, S. M. Meuer, and C. P. Bulla, "Variation associated with measurement of retinal vessel diameters at different points in the pulse cycle," *Br. J. Ophthalmol.* **88**(1), 57–61 (2004).
22. H. C. Chen, V. Patel, J. Wiek, S. M. Rassam, and E. M. Kohner, "Vessel diameter changes during the cardiac cycle," *Eye* **8**, 97–103 (1994).
23. M. J. Dumskyj, S. J. Aldington, C. J. Doré, and E. M. Kohner, "The accurate assessment of changes in retinal vessel diameter using multiple frame electrocardiograph synchronised fundus photography," *Curr. Eye Res.* **15**(6), 625–632 (1996).
24. Labsphere, *A Guide to Reflectance Coatings and Materials*, technical guide, Labsphere, North Sutton, N.H. (2002).
25. P. Viola and W. M. Wells III, "Alignment by maximization of mutual information," *Int. J. Comput. Vis.* **24**(2), 137–154 (1997).
26. J. van de Kraats, T. T. J. M. Berendschot, and D. van Norren, "The pathways of light measured in fundus reflectometry," *Vision Res.* **36**(15), 2229–2247 (1996).
27. Labsphere, *A Guide to Reflectance Coatings and Materials*, 2006 [cited: 1–25]. Available at: <http://www.labsphere.com/data/userFiles/A%20Guide%20to%20Reflectance%20Coatings%20and%20Materials.pdf>.
28. K. R. Denninghoff, R. A. Chipman, and L. W. Hillman, "Oxyhemoglobin saturation measurements by green spectral shift," *Opt. Lett.* **31**(7), 1–3 (2006).
29. F. C. Delori and K. P. Pflibsen, "Spectral reflectance of the human ocular fundus," *Appl. Opt.* **28**(6), 1061–1077 (1989).
30. M. Hammer and D. Schweitzer, "Quantitative reflection spectroscopy at the human ocular fundus," *Phys. Med. Biol.* **47**, 179–191 (2002).
31. J. M. Beach, K. J. Schwenzer, S. Srinivas, D. Kim, and J. S. Tiedeman, "Oximetry of retinal vessels by dual-wavelength imaging: calibration and influence of pigmentation," *J. Appl. Physiol.* **86**(2), 748–758 (1999).
32. K. R. Denninghoff, M. H. Smith, R. A. Chipman, L. W. Hillman, P. M. Jester, C. E. Hughes, F. Kuhn, and L. W. Rue, "Retinal large vessel oxygen saturations correlate with early blood loss and hypoxia in anesthetized swine," *J. Trauma: Inj., Infect., Crit. Care* **43**(1), 29–34 (1997).
33. F. C. Delori, "Noninvasive technique for oximetry of blood in retinal-vessels," *Appl. Opt.* **27**(6), 1113–1125 (1988).